

Mixed-Matrix Membranes Formed from Multi-Dimensional Metal–Organic Frameworks for Enhanced Gas Transport and Plasticization Resistance

Won Seok Chi,^[a] Benjamin J. Sundell,^[b] Ke Zhang,^[b] Daniel J. Harrigan,^[b] Steven C. Hayden,^[b] and Zachary P. Smith^{*[a]}

Mixed-matrix membranes (MMMs) formed by incorporating metal–organic frameworks (MOFs) into polymers have a general limitation in that the MOFs are typically formed into rather simple dimensionalities (such as 1D, 2D, or 3D). Each design approach has intrinsic—albeit independent—benefits, such as network percolation (1D), access to high-aspect ratios (2D), and ease of processability (3D). However, a design strategy is needed to combine multiple dimensionalities and, thereby, access the full range of transport and compositing benefits of these high-performance materials. Herein, a facile method to form **multi-dimensional HKUST-1 nanoparticles** is introduced by using a **modulator** to tune the **MOF nucleation and growth mechanism**. At 30 wt% multidimensional MOF loading, the MMM shows CO₂ permeabilities of approximately 2500 Barrer, which represents a 2.5-fold increase compared to that of a pure polymer without a large loss of selectivity for CO₂/CH₄ and CO₂/N₂. Additionally, almost no plasticization pressure response is observed for CO₂ up to 750 psi, suggesting an unusual stability to high activity feeds.

The chemical and petrochemical industries account for approximately 30% of worldwide energy consumption.^[1,2] Approximately half of this energy is used for separations, most notably distillation and absorption.^[1,2] With improved materials design, membranes could significantly reduce energy consumption and capital costs, thereby providing an energy-efficient alternative to traditional unit operations.^[3,4]

Presently, commercial gas-separation membranes are made almost exclusively from **polymeric materials**. However, polymers have several drawbacks including limitations in separation performance.^[5] Additionally, polymeric membranes are vulnerable to plasticization, which is an enhancement in polymer chain segmental motion in the presence of strongly sorbing molecular diluents. Plasticization often manifests as an increase

in gas permeability coupled with a significant reduction in selectivity. Owing to these drawbacks, new membrane materials are needed to enhance transport properties and reduce plasticization effects.


Much attention has focused on **mixed-matrix membranes (MMMs)**, which contain inorganic fillers dispersed in polymers to form composites. If properly designed, MMMs can have relatively good mechanical integrity compared to their purely inorganic counterparts along with superior separation performance compared to pure polymers. Moreover, they can potentially still benefit from the ease of processability of polymer-based systems.^[3] As a filler, metal–organic frameworks (MOFs) are an attractive class of crystalline materials, which are composed of metal ions or metal clusters bridged by organic ligands. These materials provide access to various structural topologies, high porosities, tunable pore sizes, and chemical features based on the selection of the specific MOF building blocks.^[6,7]

Among the hundreds of thousands of known MOFs,^[6,7] HKUST-1 is a commonly investigated MOF for MMM applications.^[8–11] **This MOF has a variety of attractive features for small molecule separations including pore channels of only 9 Å** (Figure S1, see the Supporting Information)^[12] and coordinatively unsaturated (open) metal sites, which endows this material with exceptional adsorption-based selectivities. **However**, HKUST-1 traditionally forms into three-dimensional octahedral shapes, thereby precluding ease-of-access to percolated MOF networks in MMMs. Moreover, HKUST-1 has relatively **slow nucleation rates and fast growth kinetics** that lead to large particle sizes with broad particle size distributions. **Herein**, we report a new synthetic scheme to form **multi-dimensional, branched HKUST-1 nanoparticles** using a carboxylate modulator under ambient conditions. The branched HKUST-1 nanoparticles were incorporated into a polyimide matrix, resulting in a unique and uniform structural network unlike the traditional HKUST-1 particles (bulk HKUST-1). To highlight the benefits of using branched HKUST-1 nanoparticles, MMMs formed with either bulk or branched HKUST-1 with three equivalent weight loadings were comparatively investigated in terms of structural, chemical, and gas-transport properties.

HKUST-1 particles with various structural topologies and sizes were synthesized in methanol with or without a sodium acetate modulator at room temperature for 1 h. Figure 1a shows a transmission electron microscopy (TEM) image for typical HKUST-1 particles synthesized without modulator. These particles have characteristic micron-sized dimensions (1–2 μm cross sections), octahedral morphology, and significant ag-

[a] W. S. Chi, Prof. Z. P. Smith
Department of Chemical Engineering
Massachusetts Institute of Technology
77 Massachusetts Avenue, Cambridge, Massachusetts, 02139 (USA)
E-mail: zpsmith@mit.edu

[b] B. J. Sundell, K. Zhang, D. J. Harrigan, S. C. Hayden
Aramco Services Company: Aramco Research Center
400 Technology Square, Cambridge, Massachusetts, 02139 (USA)

 Supporting Information and the ORCID identification number(s) for the author(s) of this article can be found under:
<https://doi.org/10.1002/cssc.201900623>.

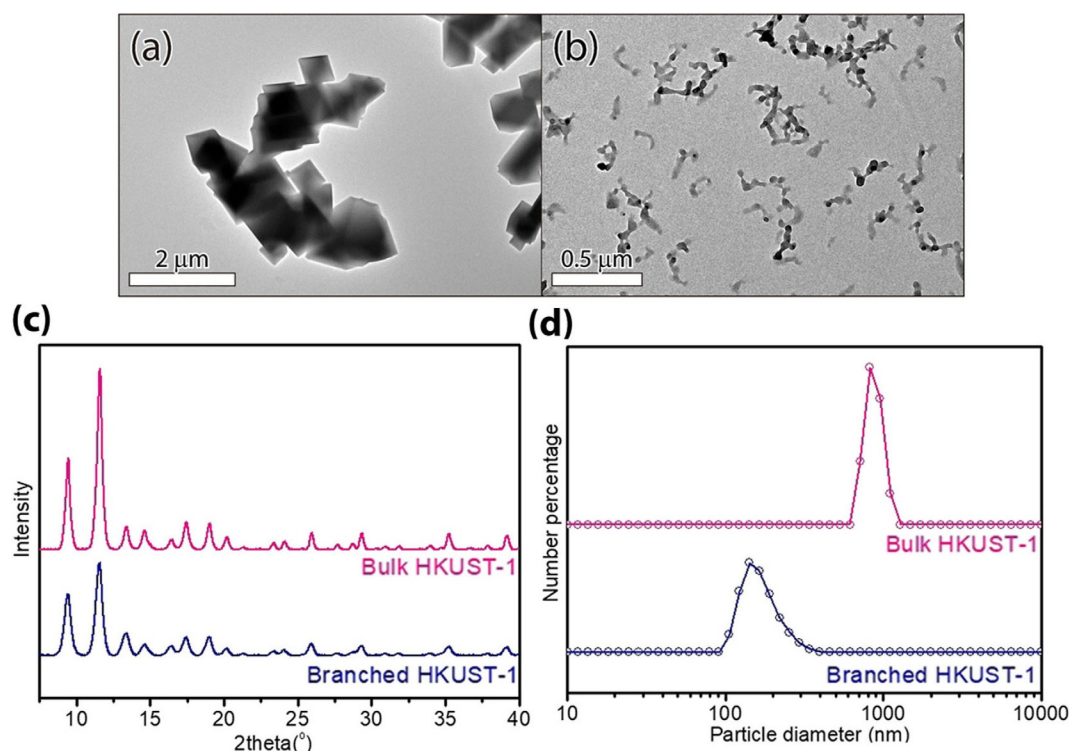


Figure 1. TEM images of (a) bulk and (b) branched HKUST-1. (c) XRD patterns, and (d) number-averaged particle size distributions of bulk and branched HKUST-1.

glomeration. Conversely, the introduction of modulator (0.3 molar equivalents to **trimesic acid**) to the HKUST-1 synthesis produces a unique branched architecture. These hierarchical HKUST-1 particles exhibit end-to-end distances of approximately 100–300 nm and branches with widths of approximately 10–30 nm, corresponding to effective aspect ratios of approximately 5–20, and a good dispersion as shown in Figure 1 b and Figure S2.

Figure 1 c presents the XRD patterns for bulk and branched HKUST-1 particles. Both bulk and branched particles show the same crystalline phase of HKUST-1. However, the branched nanoparticles show a peak width broadening indicating a smaller crystallite size.^[13,14] By applying the Scherrer equation to the dominant Bragg peak of the (222) plane,^[15] the branched nanoparticles were evaluated to have a crystallite size of around 16 nm. This feature size approximately matches the width of MOF branches as determined by TEM analysis.

Figure 1 d presents the size distributions for the bulk and branched particles as measured by using dynamic light scattering (DLS). The bulk HKUST-1 particles were measured to be approximately 1–2 μm in size, which matches the dimensions characterized by TEM. The branched HKUST-1 nanoparticles are much smaller, exhibiting diameters of approximately 100–300 nm as calculated by DLS analysis. However, notably, the particle size calculated by DLS is based on the hydrodynamic radius of a sphere.^[16] Thus, the DLS instrument measures the effective diameters of the skeletal hydrodynamic particles. These dimensions determined by DLS closely match those determined independently with TEM analysis, which cross-vali-

dates our assertion that we have formed multi-dimensional particles having small 1D inner branches encased in a 3D shell. Such structures are reminiscent of each phase in bi-continuous copolymer morphologies.^[17]

To choose the representative control (branched) and reference (bulk) samples, HKUST-1 particles with various modulator concentrations were first characterized as shown in Figures S3–S6. We performed further characterization tests on a series of HKUST-1 particles to investigate the effect of modulator concentration on the chemical structure and physical properties of the resulting MOFs. Results from Fourier-transform infrared (FTIR), Raman, and UV/Vis spectroscopy along with N₂ adsorption-desorption isotherms and thermogravimetric analysis (TGA) are provided in Figures S7–S11 and Table S1. These results indicate that the branched HKUST-1 nanoparticles have some degree of defect sites in the framework, resulting in lower surface area and adsorbate capacity owing to substituted acetates from the modulator, which replace trimesic acid.

MMMs containing the bulk (bulk MMMs) and the branched (branched MMMs) HKUST-1 were formed with various weight loadings (10, 20, and 30 wt%) using a solvent evaporation method with a controlled evaporation rate (Figure S12). For MMM fabrication, a 6FDA-DAM (6FDA = 4,4'-(hexafluoroisopropylidene)diphthalic anhydride; DAM = 2,4,6-trimethyl-1,3-phenylenediamine) polyimide was used for the polymer phase (Figure S13 and Table S1). Figure 2 a–c presents the cross-sectional field-emission scanning electron microscopy (FE-SEM) images for bulk MMMs with increasing bulk HKUST-1 loadings from 10 to 30 wt%. The bulk MMMs show an undesirable

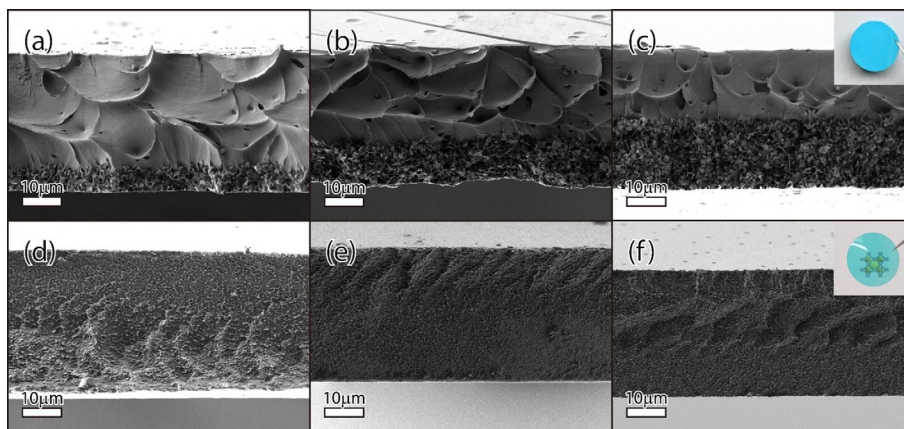


Figure 2. Cross-sectional SEM images of (a–c) bulk MMMs and (d–f) branched MMMs with various HKUST-1 weight loadings: (a,d) 10 wt%, (b,e) 20 wt%, and (c,f) 30 wt%. The insets present photos of the corresponding MMMs with 30 wt% (c) bulk and (f) branched HKUST-1 particles. A picture of the HKUST-1 crystal structure is placed behind the films to evaluate transparency.

phase-separated structure of MOF-rich and polymer-rich phases attributed to particle settling of bulk HKUST-1 that occurs during solvent evaporation. The thickness of the MOF-rich layer in the MMMs increases with increasing bulk HKUST-1 weight loading. Figure 2d–f shows the cross-sectional FE-SEM images for branched MMMs with increasing branched HKUST-1 loading from 10 to 30 wt%. Compared to their bulk counterparts, the branched HKUST-1 nanoparticles are uniformly distributed in the polyimide matrix, resulting in a homogeneous morphology across the entire film. Additionally, because of the different particle sizes and dispersion properties between bulk and branched HKUST-1, a printed picture of the HKUST-1 crystal structure is visible through the transparent branched MMM but obscured by the opaque bulk MMM in the insets of Figure 2c,f for the corresponding HKUST-1 weight loading (30 wt%). Nevertheless, it is still difficult to confirm the nanoscale morphology and dispersion characteristics for each sample from the limited resolution of FE-SEM cross-sectioning (Figure S14).

To address these limitations, **focused ion beam (FIB)-SEM** imaging was performed on bulk and branched MMMs for accurate cross-sectional analysis.^[18–20] The bulk MMMs exhibit interfacial void spaces between HKUST-1 particles and polymer (Figure S15). On the other hand, the branched MMMs show uniform HKUST-1 dispersion without any clear interfacial defects (Figure S16). Figure 3a–c shows that the 30 wt% branched MMM retains the characteristic multi-dimensional morphology. Furthermore, at these high loadings, the formation of completely isolated particle dispersions becomes somewhat frustrated, resulting in particle–particle contacts.^[21] For well-dispersed spheres, the percolation threshold, which is defined as the volume percentage of fillers required to form significant particle–particle contacts, is approximately 30 vol%.^[22] However, the branched HKUST-1 nanoparticles are not defined as true spheres in a classical sense. Instead, at a molecular level, they should be viewed as rod-like particles, therefore, requiring lower volumetric loading to achieve percolation. For ellipsoids with aspect ratios of 20, which approximately matches the highest aspect ratios for our samples, the percolation threshold

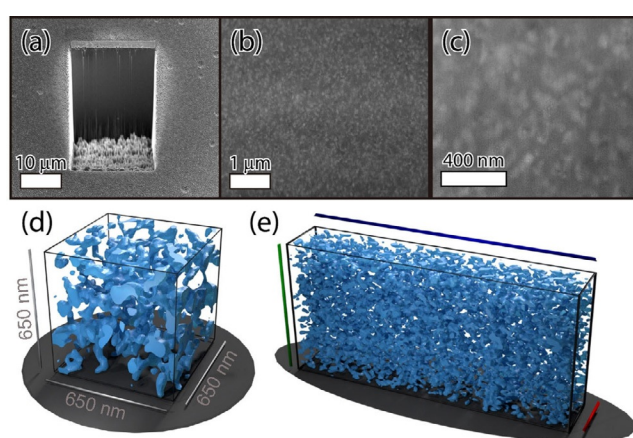


Figure 3. (a–c) FIB-SEM images of a 30 wt% branched MMM with different magnifications. 3D reconstructed images from FIB-SEM tomogram of (d) a cut-out rendering with 650 nm height, 650 nm width, and 630 nm depth; and (e) a full-scale rendering with 10.957 μm height (green bar), 29.187 μm width (blue bar), and 3.657 μm depth (red bar).

decreases by nearly a factor of 7 to approximately 4 vol%.^[22] The crystal density for HKUST-1 is approximately 1.2 g cm^{-3} ,^[9,12] and the density of 6FDA-DAM is approximately 1.3 g cm^{-3} ,^[23,24] so even at the lowest considered weight loadings (10 wt%), the branched samples have volumetric loadings above that of the estimated percolation threshold.

To further assess the connectivity of the branched HKUST-1 nanoparticles in the MMMs, we performed FIB-SEM cross-sectional tomogram for a section of the film. Figure 3d,e shows the reconstructed 3D image for a 30 wt% branched MMM under two different magnifications. The branched HKUST-1 nanoparticles form a highly interconnected nanostructured composite film, confirming the benefit of using multi-dimensional particles to more easily access percolated structures compared to other unidimensional particle approaches. Video S1 presents a video of the slice-through process for the 30 wt% branched MMM to clearly illustrate this finding. Additionally, the 3D reconstructed image is presented as an animat-

ed video in Video S2 to more clearly demonstrate the interconnected nature and uniform dispersion of the branched HKUST-1 nanoparticles in the MMM. The stability of the bulk and branched MOF dispersions in their casting solvents, and the ability of the MOF to maintain its crystalline structure during MMM film formation were further assessed using FTIR and XRD analysis, as shown in Figures S17–S19.

Gas permeation tests were performed on a pure 6FDA-DAM polymeric film along with bulk and branched MMMs with various weight loadings. The addition of bulk HKUST-1 particles in the 6FDA-DAM polymer matrix significantly increases gas permeability and decreases gas selectivity for the gas pairs of interest (CO_2/CH_4 and CO_2/N_2). For example, the 30 wt% bulk MMM shows CO_2 gas permeability of 2360 ± 80 Barrer at 15 psi, which is approximately 2.5 times higher than that of the pure 6FDA-DAM polymer (970 ± 30 Barrer). However, the CO_2/CH_4 selectivity decreases substantially from 20 ± 1 to 14.9 ± 0.7 , which is a common result for defective MMM films. Likewise, as a function of increasing HKUST-1 weight loading, the branched MMMs show a significant increase in gas permeability. As a comparison, the 30 wt% branched MMM shows a CO_2 permeability of around 2480 ± 80 Barrer at 15 psi, which is similar to that of the 30 wt% bulk MMM. However, the branched MMMs exhibit significantly smaller losses in selectivity for CO_2/CH_4 (16.5 ± 0.8) and CO_2/N_2 (16.3 ± 0.8) separations

relative to those of the pure 6FDA-DAM polymeric film ($\text{CO}_2/\text{CH}_4 = 20 \pm 1$ and $\text{CO}_2/\text{N}_2 = 17.7 \pm 0.9$). Additional details on characterization can be found in Figures S20–S25.

Effective diffusivities and solubilities were estimated for a pure 6FDA-DAM polymeric film, and bulk and branched MMMs with various weight loadings using the time-lag method (Table S4–S5).^[25] Within the resolution of these experiments, the branched MMMs exhibit a consistently increasing trend in both diffusivity and solubility for CH_4 , N_2 , O_2 , and CO_2 gases with increased loading, suggesting no noticeable defects at the interface between the branched HKUST-1 nanoparticles and the 6FDA-DAM polymer matrix. Conversely, the bulk MMMs did not exhibit any clear trend in diffusivity or solubility for CH_4 , N_2 , O_2 , or CO_2 owing to the high degree of interfacial defects.

Figure 4a,b presents the transport properties for a pure 6FDA-DAM polymeric film along with bulk and branched MMMs with various weight loadings for CO_2/CH_4 and CO_2/N_2 separations. The CO_2 gas permeability increases with increasing weight loading of the bulk and branched HKUST-1 in the MMMs. However, the branched MMMs show more limited losses in selectivity. Therefore, the property sets for the branched MMMs shift closer to the upper bound limit compared to those of the bulk MMMs. The bulk MMMs show a loss in selectivity that results in gas transport properties paralleling

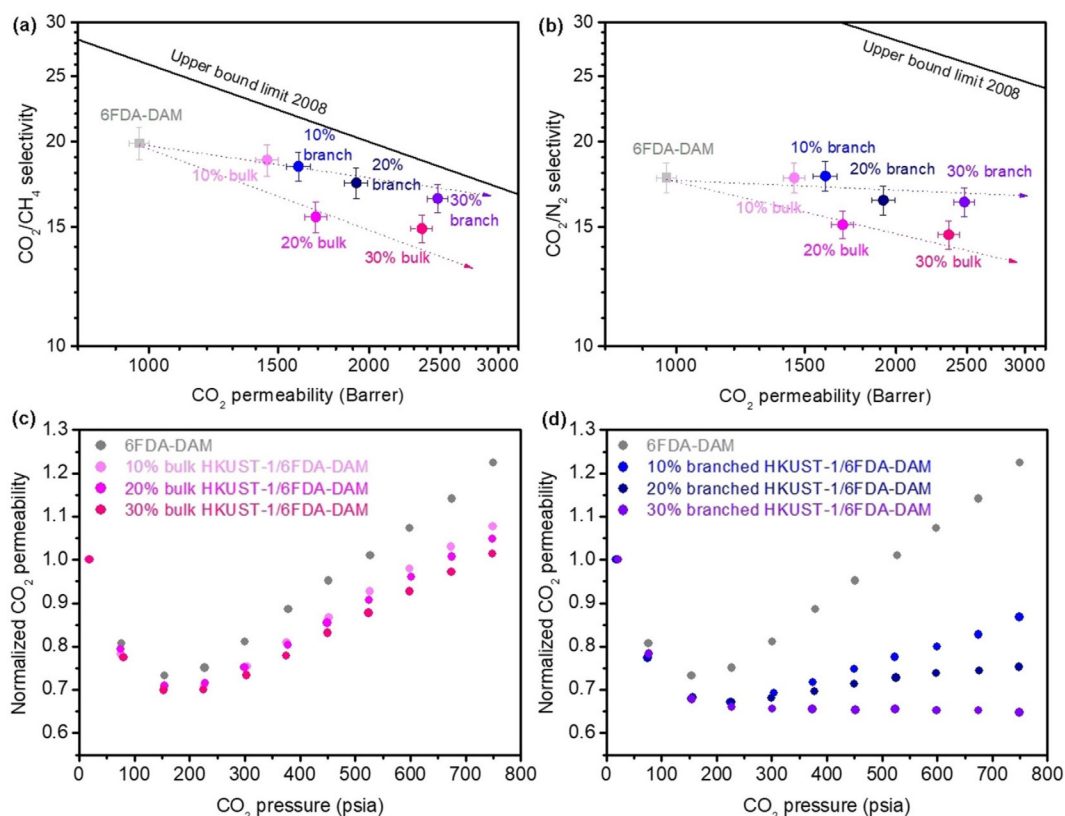


Figure 4. Gas separation performance relative to the upper bound limit for a pure 6FDA-DAM polymeric film and bulk and branched MMMs with various HKUST-1 weight loadings (10, 20, and 30 wt%) tested at 15 psi and 35 °C for (a) CO_2/CH_4 separation and (b) CO_2/N_2 separation. Normalized CO_2 permeabilities as a function of CO_2 gas pressure for (c) a pure 6FDA-DAM polymeric film, bulk MMMs, and (d) a pure 6FDA-DAM polymeric film and branched MMMs with various HKUST-1 weight loadings (10, 20, and 30 wt%).

the upper bound limit, which is characteristic of MMMs with poor interfacial compatibility.

The Maxwell model is often used to predict theoretical gas transport properties of the dispersed (filler) phase using the MMM data.^[3,26] The two basic assumptions of the model are: 1) the filler particles should be uniformly dispersed in a continuous matrix; and 2) the filler particles are spherical so that a geometrical shape factor (n) of 1/3 can be used.^[27] The first assumption requires the evaluation of permeation data at low particle loadings, in which particles are essentially surrounded by only polymer and there is no particle–particle contact. The second assumption can be relaxed for certain filler geometries such as ellipsoids.^[22]

For our samples, the addition of 10 wt% branched or bulk HKUST-1 particles to 6FDA-DAM results in gas permeabilities far beyond the limit of what is theoretically predicted by the Maxwell model. For the bulk particles, there are clear defects at the MOF–polymer interface in the MMMs which prevent the use of the Maxwell model to predict property sets. However, the branched particles are well-dispersed in the polymer without the presence of clear defects, so the inability to use the Maxwell Model requires further discussion. The high effective aspect ratio (5×20) of the branched HKUST-1 nanoparticles leads to a shape factor of less than 0.1 and a reduced percolation threshold.^[22,28] If modeled as a prolate spheroid, these aspect ratios would reduce the percolation threshold to approximately 4–16 vol%.^[22] Thus, fitting the Maxwell model with reduced shape factors did not lead to a reasonable fit because even at the lowest loading of 10 wt%, these MMMs have volumetric loadings of approximately 11 vol%, which is high enough to form a percolation network.

As a related consideration, we noticed that the branched particles have lower characteristic Brunauer–Emmett–Teller (BET) surface areas than those of the bulk particles (Tables S1). Given these differences, it is reasonable to expect that the branched particles would have reduced permeabilities compared to their bulk counterparts upon forming into MMMs. However, for all MMMs considered, the MMMs formed from branched particles showed similar or higher permeabilities than those of their bulk counterparts at equivalent weight loadings. These findings suggest that although the Maxwell model does not adequately fit our experimental results, some degree of percolation and, therefore, beneficial improvements in permeabilities at equivalent loadings can be achieved using this multi-dimensional filler strategy.

One final feature of these multi-dimensional MOFs is the unusual stability they endow their surrounding polymer to resist plasticization. To quantify this effect, Figure 4c,d shows normalized CO₂ permeabilities of a pure 6FDA-DAM polymeric film along with bulk and branched MMMs with various weight loadings. The addition of the bulk HKUST-1 to the 6FDA-DAM polymer results in a slight shift in the CO₂ plasticization pressure point, suggesting a small improvement in plasticization resistance. However, addition of the branched HKUST-1 to 6FDA-DAM results in a significant shift in the CO₂ plasticization pressure point, suggesting substantial improvements in plasticization resistance. Of note, the 30 wt% branched MMM does

not exhibit an observable plasticization pressure point up to 750 psi, indicating a highly CO₂-resistant membrane. To account for non-idealities in CO₂ permeation at high feed pressures, the CO₂ fugacity-based permeabilities and normalized CO₂ fugacity-based permeabilities of a pure polymeric film and the bulk and branched MMMs with various weight loadings are plotted in Figure S26. Although the 30 wt% loaded branched MMM does show a slightly increasing fugacity-based CO₂ permeability at high feed pressures, this effect is quite small relative to that observed for the pure polymer, indicating strong plasticization resistance of the branched MMMs. Notably, the pressures considered here represent very high activity gas-phase tests. At 750 psi and 35 °C, the estimated CO₂ activity (f/f_{sat}) is approximately 0.76. Plots of gas selectivity as a function of pressure are also included in Figure S27.

A final metric to evaluate stability is the role of CO₂ conditioning from hysteresis experiments, for which findings are presented in Figure S28(a,b). These results indicate that the branched particles more effectively hinder polymer chain mobility than their bulk counterparts through increased surface interactions between the polymer chains and the branched HKUST-1 framework. In this way, the multi-dimensional nature and small size of these nanoparticles improves the stability of their polymer supports that would otherwise not exist for separations with plasticizing gases. Furthermore, by modifying polymer chain mobility in confined spaces, the physical structure and, therefore, permeabilities of 6FDA-DAM in the branched MMMs may be fundamentally different than that of bulk 6FDA-DAM. These findings certainly support the argument of hindered polymer chain mobility, which would further prevent the clear application of the Maxwell model as discussed previously.

In summary, this study used a **modulator-based approach** to create **multi-dimensional branched structures of an HKUST-1 MOF**. These MOFs can be easily dispersed in stable casting solutions and formed into MMMs with uniform dispersions, which form a percolated network of MOFs at lower loadings than those achievable with traditional octahedral-shaped particles. Of particular interest, no filler-particle alignment is required as is the case with 1D and 2D materials. Designing multi-dimensional structures presents new opportunities for using MOFs in MMMs, particularly using interconnected- and branched-MOF particles as a means to surpass traditional transport and stability limitations at lower loadings for MMMs with opportunities for using these strategies broadly for real-world and industrially relevant separations.

Acknowledgements

This research was supported through a Research Agreement with Saudi Aramco, a Founding Member of the MIT Energy Initiative. The authors wish to thank Austin Akey and the Harvard Center for Nanoscale Sciences, part of the NSF National Nanotechnology Infrastructure Network (NNIN), for help with acquisition and interpretation of SEM data.

Conflict of interest

The authors declare no conflict of interest.

Keywords: gas separation • HKUST-1 • metal–organic framework • mixed-matrix membranes • plasticization

- [1] D. S. Sholl, R. P. Lively, *Nature* **2016**, 532, 435–437.
- [2] D. Gielen, *Tracking industrial energy efficiency and CO₂ emissions*, International Energy Agency Report, **2007**.
- [3] M. Galizia, W. S. Chi, Z. P. Smith, T. C. Merkel, R. W. Baker, B. D. Freeman, *Macromolecules* **2017**, 50, 7809–7843.
- [4] R. W. Baker, K. Lokhandwala, *Ind. Eng. Chem. Res.* **2008**, 47, 2109–2121.
- [5] L. M. Robeson, *J. Membr. Sci.* **2008**, 320, 390–400.
- [6] M. Eddaoudi, J. Kim, N. Rosi, D. Vodak, J. Wachter, M. O’Keeffe, O. M. Yaghi, *Science* **2002**, 295, 469–472.
- [7] O. M. Yaghi, M. O’Keeffe, N. W. Ockwig, H. K. Chae, M. Eddaoudi, J. Kim, *Nature* **2003**, 423, 705–714.
- [8] J. B. DeCoste, M. S. Denny, Jr., G. W. Peterson, J. J. Mahle, S. M. Cohen, *Chem. Sci.* **2016**, 7, 2711–2716.
- [9] S. Basu, A. Cano-Odena, I. F. J. Vankelecom, *J. Membr. Sci.* **2010**, 362, 478–487.
- [10] R. Lin, L. Ge, H. Diao, V. Rudolph, Z. Zhu, *ACS Appl. Mater. Interfaces* **2016**, 8, 32041–32049.
- [11] S. Kanehashi, G. Q. Chen, C. A. Scholes, B. Ozcelik, C. Hua, L. Ciddor, P. D. Southon, D. M. D’Alessandro, S. E. Kentish, *J. Membr. Sci.* **2015**, 482, 49–55.
- [12] S. S.-Y. Chui, S. M.-F. Lo, J. P. H. Charmant, A. G. Orpen, I. D. Williams, *Science* **1999**, 283, 1148–1150.
- [13] H. P. Klug, L. E. Alexander, *X-Ray Diffraction Procedures: For Polycrystalline and Amorphous Materials*, 2nd ed., Wiley, Chichester, **1974**.
- [14] J. E. Bachman, Z. P. Smith, T. Li, T. Xu, J. R. Long, *Nat. Mater.* **2016**, 15, 845–849.
- [15] A. L. Patterson, *Phys. Rev.* **1939**, 56, 978–982.
- [16] B. J. Berne, R. Pecora, *Dynamic Light Scattering: With Applications to Chemistry, Biology, And Physics*, Wiley, Chichester, **1976**.
- [17] N. Zhou, F. S. Bates, T. P. Lodge, *Nano Lett.* **2006**, 6, 2354–2357.
- [18] T. Rodenas, I. Luz, G. Prieto, B. Seoane, H. Miro, A. Corma, F. Kapteijn, F. X. Llabrés i Xamena, J. Gascon, *Nat. Mater.* **2015**, 14, 48–55.
- [19] T. Rodenas, M. van Dalen, E. García-Pérez, P. Serra-Crespo, B. Zornoza, F. Kapteijn, J. Gascon, *Adv. Funct. Mater.* **2014**, 24, 249–256.
- [20] L. A. Giannuzzi, F. A. Stevie, *Introduction to Focused Ion Beams*, Springer, Berlin, **2005**.
- [21] R. W. Baker, *Membrane Technology and Applications*, 3rd ed., Wiley, Chichester, **2012**.
- [22] E. J. Garboczi, K. A. Snyder, J. F. Douglas, M. F. Thorpe, *Phys. Rev. E* **1995**, 52, 819–828.
- [23] J. H. Kim, W. J. Koros, D. R. Paul, *Polymer* **2006**, 47, 3094–3103.
- [24] W. Xu, D. R. Paul, W. J. Koros, *J. Membr. Sci.* **2003**, 219, 89–102.
- [25] H. L. Frisch, *J. Phys. Chem.* **1957**, 61, 93–95.
- [26] J. C. Maxwell, *A Treatise on Electricity and Magnetism*, Clarendon, Oxford, **1881**.
- [27] R. H. B. Bouma, A. Checchetti, G. Chidichimo, E. Drioli, *J. Membr. Sci.* **1997**, 128, 141–149.
- [28] J. Fukushima, S. Tsubaki, T. Matsuzawa, K. Kashimura, T. Mitani, T. Namio-ka, S. Fujii, N. Shinohara, H. Takizawa, Y. Wada, *Materials* **2018**, 11, 169.

Manuscript received: March 1, 2019

Accepted manuscript online: March 11, 2019

Version of record online: April 29, 2019